Chapter 2

Quantum Dot-Semiconductor Optical Amplifiers (QD-SOA): Dynamics and Applications

Yossef Ben Ezra and Boris I. Lembrikov

Additional information is available at the end of the chapter

http://dx.doi.org/10.5772/intechopen.74655

Abstract

Quantum dot-semiconductor optical amplifiers (QD-SOA) attracted strong interest for applications in optical communications and in all-optical signal processing due to their high operation rate, strong nonlinearity, small gain recovery time of about few picoseconds, broadband gain, low injection current and low noise figure (NF). In this chapter, we present the theoretical investigation of the gain recovery time acceleration in DQ SOA; the specific features of the cross gain modulation (XGM) in QD-SOA; the influence of the optical injection on the dynamics of QD-SOA based on the QD in a well (QDWELL) structure. We describe the following applications of QD-SOA: the all-optical ultra-wideband (UWB) pulse generation based on the Mach-Zehnder interferometer (MZI) with a QD-SOA; the ultra-fast all-optical signal processor based on QD-SOA-MZI; the ultra-fast all-optical memory based on QD-SOA. The contents of the chapter are mainly based on the original results.

Keywords: quantum dot, semiconductor optical amplifier, cross-gain modulation, all-optical processor, all-optical radio signal generation

1. Introduction

Quantum dot-semiconductor optical amplifiers (QD-SOA) are characterized by ultrafast gain recovery time (GRT) of the order of magnitude of several picoseconds, broadband gain, low noise figure (NS), high saturation output power, and high four-wave mixing (FWM) efficiency [1]. QD-SOA can be used as ultra-wideband (UWB) polarization-insensitive high-power amplifiers, high-speed signal regenerators, and wideband wavelength converters (WC) [1–5]. These unique features of QD-SOA are essentially due to the concentration of the injected electrons and holes into nanosized QD [1]. QD is a nanostructure characterized by the electron

and hole confinement in all three dimensions [2, 6]. QD is a cluster with the dimensions of several nanometers made of a semiconductor material [2]. In a QD charge carriers occupy a limited number of energy levels similarly to an atom, and the density of states is quantized [2]. As a result, QD has freedom of a wavelength choice [1]. A QD contains hundreds of thousands of atoms [2]. Typically, III-V QD are epitaxially grown on a semiconductor substrate [2]. The process of the spontaneous formation of three-dimensional islands during strained layer epitaxial growth is known as the Stranski-Krastanov mechanism [2]. A continuous film of a quantum well (QW) thickness lies underneath QD, and it is called the wetting layer (WL) [2]. The lattice constant of the deposited semiconductor material must be larger than that of the substrate [2]. For instance, an InAs film with the lattice constant of 6.06 Å can be deposited on a GaAs substrate with the lattice constant of 5.64 Å or on an InP substrate with the lattice constant of 5.87 Å [2]. Stranski-Krastanov grown QD typically has a pyramidal shape with a base of 15–20 nm and a height of about 5 nm; the QD density per unit area is between 10^9 and 10^{12} cm^{-2} [1, 2]. The methods of the QD energy levels and density of states evaluation are presented in Ref. [6].

The theory of the optical signal amplification and processing based on the density matrix equations for the electron-light interaction and the optical pulse propagation equations has been developed [7]. The QD spatial localization, the inhomogeneous spectral broadening caused by the QD size, shape, composition, and stain distribution, the carrier capture from WL, the carrier emission to WL, intradot population relaxation, and homogeneous spectral broadening have been taken into account, and the nonlinear optical response has been also investigated [7]. The phenomenological approach to the QD-SOA theory is based on the system of rate equations for photons and charge carriers in QD [2, 5, 8]. In such a case, the QD is considered as a three-state system including the ground state (GS), the excited state (ES) and WL [2, 5, 8]. The electron dynamics in QD is assumed to be slower than the hole dynamics, and for this reason, only the rate equations for electron populations of GS, ES and WL are included in the dynamic model [2, 5, 8]. Using this model, we investigated theoretically acceleration of gain recovery and dynamics of electrons in QD-SOA [9, 10]. We have shown that the QD-SOA GRT may be substantially decreased, and the patterning effect is reduced by increasing the optical pump power, while the chirp in QD-SOA is about one order of magnitude lower than the one in the bulk SOA [9, 10]. We studied theoretically the cross-gain modulation (XGM) process in QD-SOA taking into account the QD-SOA inhomogeneous spectral broadening [11]. We have shown that XGM in QD-SOA occurs at larger detuning between the pump and signal light waves as compared to the bulk SOA, the asymmetric chirp may be diminished by the bias current increase, and XGM process slows down in the nonlinear regime [11].

Recently, QD-SOA and lasers based on a novel quantum dot-in-a-well (QDWELL) structure have been proposed where the self-assembled QD has been grown into QW with the discrete energy levels and the two-dimensional (2D) electron gas instead of ordinary QD laser and SOA with the continuous carrier energy in WL [12, 13]. The operation of QD-SOA based on a QDWELL structure (QDWELL SOA) has been investigated both theoretically and experimentally [12–16]. The complicated dynamics of QDWELL SOA is described by the system of the rate equations for the electrons and holes in QD and QW including the strongly nonlinear electron and hole scattering rates for the carrier scattering between QD and QW [12, 17]. The

operation rate of QDWELL SOA is limited by the desynchronized recovery dynamics of electrons and holes caused by the different microscopic scattering rates [15]. We have shown theoretically that the electron and hole dynamics in QDWELL lasers and SOA can be synchronized by a sufficiently strong optical injection and consequently the QDWELL lasers and SOA performance including the operation rate can be significantly improved [18–22].

Optical signal processing is based on the linear and nonlinear optical techniques for the digital, analogous and quantum information [23]. It is a promising technology for increasing the processing speed of devices, the capacity of optical links, and reducing of energy consumption [23]. In particular, QD-SOA are excellent candidates for high-speed data and telecommunication applications due to their ultrafast gain dynamics and pattern effect-free amplification [15]. We proposed the following novel applications of QD-SOA in optical communications:

1. a novel all-optical method of the impulse radio ultra-wideband (IR-UWB) pulse generation based in an integrated Mach-Zehnder interferometer (MZI) with QD-SOA as an active element inserted into one arm of the integrated MZI [24–26];
2. an ultra-fast all-optical processor based on QD-SOA [27, 28]; and
3. an ultra-fast all-optical memory based on QD-SOA [29, 30].

The detailed results of the numerical simulations are presented in Refs. [9–11, 18–22, 24–30]. In this work, we discuss the theoretical models of QD-SOA, QDWELL SOA, and some devices for the all-optical signal processing, summarize the results obtained and present the necessary numerical estimations. The chapter is organized as follows. In Section 2, we discuss the dynamics of the gain recovery and XGM processes in QD-SOA. In Section 3, we consider the influence of the optical injection on the QDWELL SOA performance. The applications of QD-SOA in optical signal processing are discussed in Section 4. The conclusions are presented in Section 5.

2. Specific features of the QD-SOA dynamics

2.1. Theoretical model of QD-SOA

In this section, we theoretically investigate the gain recovery process and XGM in QD-SOA. The analysis is based on the simultaneous solution of the rate equations for the electron density per unit volume in WL N_w, electron occupation probabilities f and h of GS and ES, respectively, and the equations for pump and signal wave photon densities $S_{p,s}$ and phases $\theta_{p,s}$ [9–11]. The energy band structure of QD-SOA is shown in **Figure 1**.

The carrier transitions between WL, ES and GS are characterized by different relaxation times. The fast transition processes between WL and ES, and between ES and GS are described by the relaxation times $\tau_{w2}, \tau_{21}, \tau_{12} \sim \left(10^{-12} - 10^{-11}\right)s$ [5, 8]. The transitions from ES to WL are characterized by the much larger carrier escape time $\tau_{2w} \sim 10^{-9}s$ [5]. The rate equations for the spatially averaged over the QD-SOA length L values of N_w, f, h have the form [5, 8–11]:

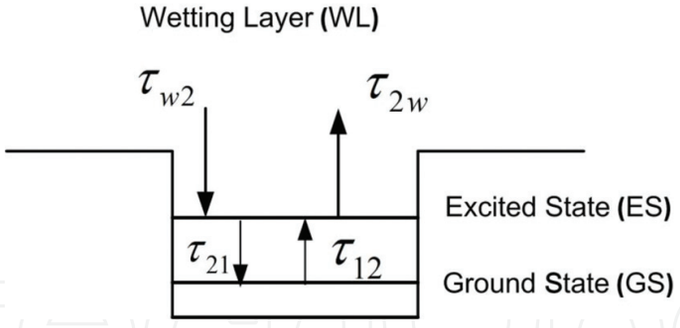

Figure 1. The QD-SOA energy band structure.

$$\frac{\partial N_w}{\partial t} = \frac{J}{eL_w} - \frac{N_w(1-h)}{\tau_{w2}} + \frac{N_w h}{\tau_{2w}} - \frac{N_w}{\tau_{wR}} \tag{1}$$

$$\frac{\partial h}{\partial t} = \frac{N_w L_w (1-h)}{N_Q \tau_{w2}} - \frac{N_w L_w h}{N_Q \tau_{2w}} - \frac{(1-f)h}{\tau_{21}} + \frac{f(1-h)}{\tau_{12}} \tag{2}$$

$$\frac{\partial f}{\partial t} = \frac{(1-f)h}{\tau_{21}} - \frac{f(1-h)}{\tau_{12}} - \frac{f^2}{\tau_{1R}} - \frac{g_p Lc}{N_Q\sqrt{\varepsilon_r}}(2f-1)S_p - \frac{g_s Lc}{N_Q\sqrt{\varepsilon_r}}(2f-1)S_s \tag{3}$$

The equations for $S_{p,s}$ and $\theta_{p,s}$ are given by [8–11, 31]:

$$\frac{\partial S_{p,s}(z,\tau)}{\partial z} = \left(g_{p,s} - \alpha_{\text{int}}\right) S_{p,s}(z,\tau) \tag{4}$$

$$\frac{\partial \theta_{p,s}}{\partial z} = -\frac{1}{2}\alpha g_{p,s} \tag{5}$$

Here, J is the bias current density, N_Q is the QD density per unit area, L_w is the effective thickness of the active layer, τ_{wR}, τ_{1R} are the spontaneous lifetime in WL and QD, respectively, c is the free space light velocity, e is the electron charge, ε_r is the active layer permittivity, α_{int} is the absorption coefficient of the QD-SOA material, α is the linewidth enhancement factor (LEF), $\tau = t \mp z/v_g$ is the temporal variable related to the wave propagation in a retarded frame, $v_g = c/n_g$ is the light group velocity, n_g is the group refraction index, $S_{p,s} = P_{p,s}/\left(\hbar\omega_{p,s}\left(v_g\right)_{p,s}A_{eff}\right)$, $P_{p,s}$ are the pump and signal wave power, $\hbar = h/2\pi$, h is the Planck constant, A_{eff} is the QD-SOA effective cross-section, $g_{p,s}$ are the pump and signal wave modal gains. They are given by [31]:

$$g_{p,s}(\omega_0) = \frac{2\Gamma N_Q}{a}\int d\omega F(\omega)\sigma(\omega_0)(2f-1) \tag{6}$$

where Γ is the confinement factor which is the same for both light waves, a is the mean size of QD, factor 2 takes into account the spin degeneracy of the QD levels, $F(\omega)$ is the Gaussian

distribution of the transition frequency. It is related to the inhomogeneous broadening, and it has the form [31]:

$$F(\omega) = \frac{1}{\Delta\omega\sqrt{\pi}} \exp\left[-\frac{(\omega - \overline{\omega})^2}{(\Delta\omega)^2}\right] \tag{7}$$

where $\overline{\omega}$ is the average transition frequency, $\Delta\omega$ is related to the inhomogeneous linewidth $\gamma_{in\text{hom}}$ as follows: $\gamma_{in\text{hom}} = 2\sqrt{\ln 2}\Delta\omega$ [31]. Typically, the inhomogeneous broadening of QD lasers and SOA σ_E is about 30–40 meV and the homogeneous broadening is about 15–20 meV at room temperature [3]. The QD device inhomogeneous broadening has both advantages and disadvantages for different applications. The generation, propagation, and amplification of ultrafast pulses can be realized due to the wide bandwidth [2]. On the other hand, the inhomogeneous broadening caused by the QD size fluctuations increases the transparency current and reduces the modal and differential gain [2]. The cross-section $\sigma(\omega_0)$ of interaction of photons of frequency ω_0 with the carriers in QD at the transition frequency ω is given by [31]:

$$\sigma(\omega_0) = \sigma_{res} \frac{1}{\left[1 + (\omega - \omega_0)^2 T_2^2\right]} \tag{8}$$

The cross-section $\sigma(\omega_0)$ at the frequency $\omega = \omega_0$ has its maximum value of the resonant cross section σ_{res} which has the form [31]:

$$\sigma_{res} = \frac{\mu^2 \omega_0 T_2}{c n_g \varepsilon_0 \hbar} \tag{9}$$

where μ is the dipole moment of the optical transition, $T_2 = 2\gamma_{\text{hom}}^{-1}$ is the dephasing time related to the homogeneous linewidth γ_{hom}, ε_0 is the free space permittivity.

In our analysis of the QD-SOA dynamics, we are interested in the temporal dependence of the power $P_{p,s}$ and phase $\theta_{p,s}$ of the lightwave pulses with the bit rates $B \leq 40\ Gb/s$ at the output of the QD-SOA [9–11]. In such a case, the lightwave radiation is filling the QD-SOA active region of the length $L \sim 1\ mm$ and interacts with all QD. For this reason, the light intensity can be averaged over the QD-SOA length L [9–11]. Integrating Eq. (4) over z and averaging the result over the QD-SOA active region length L, we obtain [11]:

$$S_{p,s}(\tau) = \frac{1}{L}\left(S_{p,s}(\tau)\right)_{in} \int_0^L dz \exp\left[\int_0^z \left(g_{p,s} - \alpha_{\text{int}}\right) dz'\right] \tag{10}$$

Integrating Eq. (5), we obtain the phases $\theta_{p,s}$ [11]:

$$\theta_{p,s} = -\frac{\alpha}{2} \int_0^L g_{p,s} dz \tag{11}$$

The chirp $\delta\nu_{p,s}$ is given by [11]:

$$\delta\nu_{p,s} = -\frac{1}{2\pi}\frac{\partial\theta_{p,s}(\tau)}{\partial\tau} \tag{12}$$

System of Eqs. (1)–(3) with the average pump and signal photon densities (10) describes the gain recovery and XGM processes in QD-SOA. These equations are strongly nonlinear, and for this reason, they are extremely complicated. Their analytical solution in a closed form is hardly possible. We solved the system of Eqs. (1)–(5) numerically for the following typical values of the material parameters: $L = 2\ mm$, $L_w = 0.1 - 0.2\ \mu m$, the QD-SOA width $W = 10\ \mu m$, $\Gamma \sim 3 \times 10^{-2}$, $\tau_{w2} = 3\ ps$, $\tau_{21} = 0.16\ ps$, $\tau_{12} = 1.2\ ps$, $\tau_{1R} = 0.4\ ns$, $\tau_{2w} = \tau_{wR} = 1\ ns$, $N_Q = 5\times 10^{10}\ cm^{-2}$, $g_{\max} = 11.5\ cm^{-1}$, $\sigma_E = 30\ meV$, $\tau_{12} = \tau_{21}\rho\exp(\Delta E_{21}/k_BT)$, $\rho = 1$, $\alpha_{\text{int}} = 3\ cm^{-1}$, $\alpha = 0.1$, the energy separation between ES and GS $\Delta E_{21} = 30\ meV$, the temperature $T = 300\ K$, k_B is the Boltzmann constant [5, 8, 31, 32]. The simulation results for the case of the QD-SOA gain recovery process [9, 10] and XGM in QD-SOA [11] are discussed in subsections 2.2 and 2.3, respectively.

2.2. Theoretical analysis of the gain recovery process in QD-SOA

The QD-SOA performance is mainly determined by their GRT and the magnitude of the chirp $\delta\nu_{p,s}$. GRT is limited by the carrier lifetime which can be decreased by the increase of the applied bias current and the light intensity in the active layer of SOA [9, 10]. Consider first the two lightwaves with the same wavelength $\lambda = 1550\ nm$ inserted into the QD-SOA: a continuous wave (CW) probe lightwave and a pump lightwave representing a Gaussian pulse with a full-width of half maximum (FWHM) of 150 fs [9]. In such a case, the numerical simulation results for the probe power $P_p = 10\mu W$ and the bias current of 20 mA show that the 10–90% GRT is about 378 fs, which is comparable to the experimental results for SOA based on self-assembled InAs-InGaAS QD [2, 33, 34]. It is much smaller than the GRT of about 100 ps for the QW SOA and several hundred ps for the bulk SOA [2, 35]. The low GRT in QD-SOA is related to the small electron transition time from ES to GS $\tau_{21} \sim 10^{-1}\ ps$. The GRT decreases with the increase of the input probe wave power $P_{p,in}$ due to the high stimulated transition rates [9]. The chirp (12) increases with the increase of $P_{p,in}$ due to the increase of the photo carrier density, which results in a larger change of the QD-SOA refractive index Δn [9].

Consider now the influence of the bias current and the CW probe optical wave intensity on the QD-SOA dynamics in two cases of the optical signal wave with the power of $P_s = 1\ mW$, wavelength $\lambda = 1550\ nm$ and a bit rate $B = 40\ Gb/s$: (1) the pseudorandom bit sequence (PRBS) of the length $\left(2^{11} - 1\right)$; (2) the Gaussian pulse with FWHM $T_0 = 15\ ps$ [10].

We start with the analysis of the QD-SOA dynamics in the absence of the probe optical wave. In the PRBS case, the simulation results show that at a low bias current of an order of magnitude of $I = 10\ mA$ close to the transparency value of about 6 mA, the patterning effect is strongly pronounced. In such a case, the QD-SOA does not respond adequately to the fast changes of the input optical signal. The electron exchange processes between WL and ES are

substantially slower than the transitions between ES and GS. As a result, only the GS electron occupation probability $f(t)$ follows the PRBS. The rise time of the WL electron density $N_w(t)$ coincides with time duration of long pulses $\Delta t_r \sim 100\ ps$ since it is determined by $\tau_{2w} = 1\ ns$. On the contrary, the decrease of $N_w(t)$ determined by the faster electron transitions from WL to ES is characterized by the short characteristic time $\Delta t_d \sim \tau_{w2} \sim 10^{-12}\ s$ [10]. The QD-SOA dynamics for the Gaussian pulse at the low bias current is similar since the recovery times for the dynamic variables are quite different: it is about 50 ps for $N_w(t)$, 25 ps for $h(t)$, and 17 ps for $f(t)$ [10]. The pulse broadening for each one of the dynamic variables is different which results in the patterning effect. For the bias current $I = 30\ mA$ which is much larger than the transparency current, the strong injection of the charge carriers increases the ES population and the number of fast transitions from ES to GS with a characteristic timescale of $\tau_{12} \sim 1\ ps$. These fast transitions become dominant. However, the WL population dynamics determined by slow processes does not change significantly. For this reason, the patterning effect decreases for large bias current, but it still exists [10]. The numerical simulation results show that in the absence of the optical probe wave the increase of the bias current does not improve significantly the QD-SOA performance both for the Gaussian pulse and for the PRBS signal [10]. Consider now the influence of the counter-propagating strong probe wave with the power $P_p \sim 1\ mW$ and wavelength $\lambda = 1535\ nm$ on the QD-SOA carrier dynamics [10]. This optical injection gives rise to the stimulated emission between the GS and the valence band. Consequently, the transitions from ES to GS accelerate, the ES population is rapidly decreasing, and the fast transitions from WL to ES characterized by $\tau_{w2} = 3\ ps$ become dominant. The numerical simulation results show that in such a case, the changes of $N_w(t), h(t), f(t)$ do not exceed 10%, GRT is about 15 ps, the pulse broadening and the delay time are approximately the same for all dynamic variables $N_w(t), h(t), f(t)$, and the patterning effect completely vanishes [10]. At probe wave, power of several milliwatts and FWHM of 150 fs, the GRT reduces to 0.2 ps since the GRT lower limit is determined by the QD-SOA lowest transition time between ES and GS $\tau_{21} = 0.16\ ps$. GRT of 39 ps in the bulk SOA has been demonstrated experimentally for the optical injection power of 100 mW, or by the bias currents of 150–450 mA without optical injection [35].

2.3. Peculiarities of XGM in QD-SOA

Consider now the peculiarities of XGM in QD-SOA caused by the gain inhomogeneous broadening which is due to the variation of QD size, shape, and local strain [11]. XGM is an essentially nonlinear process in SOA caused by the carrier density change influence on the input signal waves [36]. Typically, XGM in SOA may realize the wavelength conversion [36]. The XGM process in QD-SOA involves three types of transitions: (1) fast transitions between ES and GS characterized by $\tau_{21}, \tau_{12} \sim (0.1 - 1)\ ps$; (2) intermediate timescale transitions from WL to ES with the relaxation time τ_{w2} of several picoseconds; (3) slow escape transitions from ES to WL determined by the spontaneous recombination time in WL $\tau_{wR} = \tau_{2w} \sim 1\ ns$. We investigated theoretically the wavelength conversion in QD-SOA for the CW pump wave with the power $P_p = 0.1\ mW$ and the wavelength $\lambda_p = 1530\ nm$ and the input PRBS nonreturn-to-zero (NRZ) signal of the length $2^{11} - 1$ with the wavelength $\lambda_p = 1550\ nm$. We solved

numerically system of Eqs. (1)–(3) with the modal gains $g_{p,s}$ (6), the average photon densities $S_{p,s}$ (10), phases $\theta_{p,s}$ (11) and the typical values of the material parameters mentioned in subsection 2.1 [11]. For the sake of definiteness, we consider the counter-propagating signal and pumping waves [11]. A schematic diagram of the traveling wave (TW) QD-SOA is shown in **Figure 2**.

We used the bias current values $I = 10\ mA$, $I = 30\ mA$, and the bit rates of 10, 40 Gb/s [11]. We start with the analysis of the bias current, the optical power, and the signal bit rate influence on the XGM in QD-SOA. The numerical simulation results show that at the low input signal power level $P_s = 0.1\ mW$ and $I = 30\ mA$, QD-SOA operates close to the linear regime where $f \approx 1$ and the variations of the ES and GS populations of about 10–20% are relatively small [11]. However, in the linear regime, the population exchange between ES and GS is sufficient for the required level of XGM. In the nonlinear regime corresponding to the strong enough signal wave power $P_s = 10\ mW$, an additional number of electrons in GS is necessary for maintaining the gain level. As a result, the electron concentration N_w in WL reduces to about 30% of its maximum value; WL refilling is necessary, and the slow transitions between ES and WL become essential. The XGM process is slowing down [11].

Consider now the temporal dependence of the input signal power P_s and the output power P_s^{out}. The patterning effect is strongly pronounced for the bit rate of 10 Gb/s and a low bias current $I = 10\ mA$, and it becomes even stronger for the bit rate of 40 Gb/s. The patterning effect can be reduced by the increase of the bias current for comparatively low bit rates. Indeed, for the increased bias current $I = 30\ mA$ and for the bit rate of 10 Gb/s, the patterning effect practically vanishes. However, at higher bit rate of 40 Gb/s, the increase of the bias current does not reduce the patterning effect because the QD-SOA operation rate is still limited

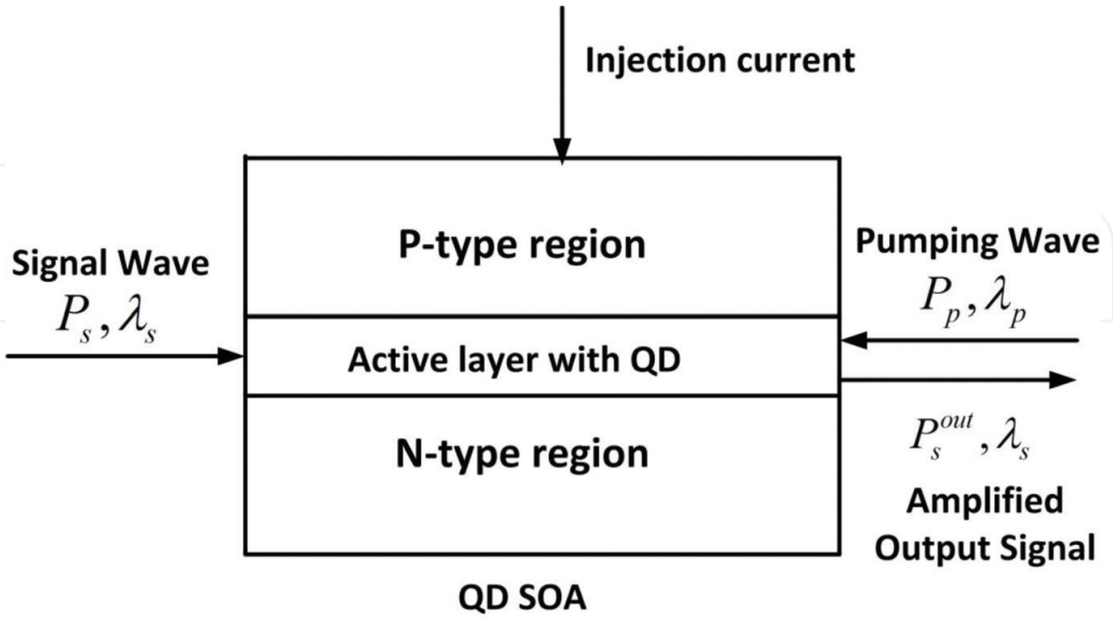

Figure 2. Schematic diagram of the traveling wave (TW) QD-SOA with the counter-propagating signal and pumping optical waves.

by the comparatively slow processes in WL. The chirp $\delta\nu_{p,s}$ evaluated according to Eq. (12) increases substantially up to 20 GHz for the bias current $I = 30\ mA$ and the bit rate of 40 Gb/s, and it is strongly asymmetric with the magnitude of the negative chirp substantially larger than the positive one [11].

Consider the possibility of XGM in QD-SOA between the waves with the detuning larger than the QD-SOA homogeneous broadening. In such a case, we divide QD into groups with different resonant frequencies caused by the inhomogeneous broadening. This time, we solve Eqs. (1)–(3) numerically for the QD group 1 and 2 with a detuning substantially larger than the QD-SOA homogeneous broadening [11]. The numerical simulation results show that the strong interaction through WL for these QD groups occurs for a comparatively low bit rate of 10 Gb/s and significantly diminishes at 40 Gb/s. At the large bit rates, the ES and GS populations of the first QD group do not follow the changes of the ES and GS populations of the second QD group, the WL electron concentration is slightly varying, and the XGM effect vanishes. The output optical power P_{out} and the output signal chirp correlate with the input power for the bit rate of 10 Gb/s, but they do not correlate anymore for the bit rate of 40 Gb/s.

The comparison of the performance of bulk, multiquantum well (MQW) and QD-SOA shows that XGM can be realized in the bulk SOA for the bias current of $(160 - 200)\ mA$, in MQW SOA for the bias current of $(30 - 150)\ mA$, while in QD-SOA, similar results for XGM can be achieved for the bias current of $30\ mA$ (see [11] and references therein). The bulk and MQW SOA performance significantly deteriorates at the bit rates of about 10 Gb/s because of the large radiative relaxation time. On the ontrary, the pattern-effect-free XGM in QD-SOA is possible at 10 Gb/s due to the small relaxation time $\tau_{21} \sim 10^{-1}\ ps$: $\tau_{21}^{-1} \gg B = 10\ Gb/s$. XGM in the columnar QD (CQD) SOA at the wavelength of 1550 nm has been demonstrated experimentally [37]. CQD-SOA based on near isotropically shaped CQD make possible polarization-independent WC [37]. It has been shown in particular that the bit rate of 40 Gb/s is cut-off transmission capacity for the distortion-free XGM wavelength conversion [37].

3. The influence of the optical injection on the QDWELL SOA performance

In this section, we consider XGM in the TW QDWELL SOA mainly following references [20–22].

The block diagram of the TW QDWELL SOA is presented in **Figure 3**. Typically, a QDWELL active region structure consists of 10–15 InGaAs quantum well (QW) layers with a height of about 4 nm containing embedded InAs QD with a size of approximately 4 nm x 18 nm x 18 nm [12]. The layers of InGaAs/InAS QD are separated by 33 nm GaAS spacers providing the strain relaxation between successive QD layers [13]. The electric bias current is injected into the QW layers which represent the reservoir of the 2D carrier gas unlike the WL with the continuous energy of carriers in ordinary QD-SOA [12]. The ridge width and the waveguide length are $2 - 4\ \mu m$ and $1 - 2\ mm$, respectively [13]. The co-propagating optical signal and pumping waves with the power $P_{p,s}$ and wavelength $\lambda_{p,s}$ are fed into the QDWELL SOA. GS is in the

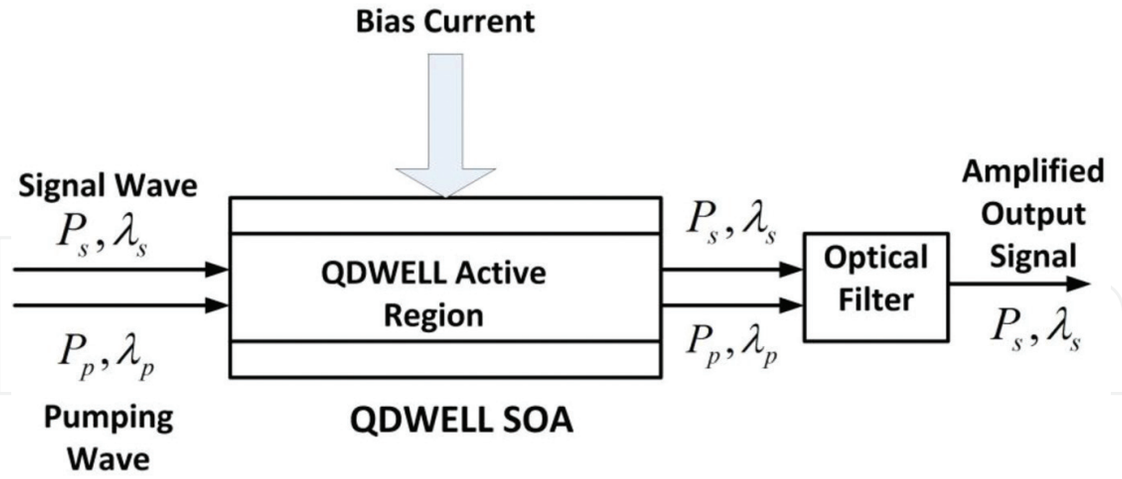

Figure 3. The block diagram of the TW QDWELL SOA with the co-propagating optical signal wave (P_s, λ_s) and pumping wave (P_p, λ_p).

resonance with the signal wave to be amplified [13]. The GS is filled by the carriers from ES and QW carrier reservoir [13]. The fast transitions between ES and GS provide the ultrafast GS recovery time of about 130 *fs*, the scattering time from the QW into the QD is about $1-2$ *ps*, and the time of slow recovery of the QW reservoir after depletion is about $100-150$ *ps* [13]. As a result, the maximum frequency bandwidth of the QW carrier reservoir is about $7-10$ *GHz* while the fast QD dynamics bandwidth is beyond 100 *GHz* [13]. The QDWELL SOA dynamics is described by the system of Lüdge-Schöll (LS) rate equations for the electron and hole occupation probabilities $\rho_{e,h}$ in the confined GS of QD and for the electron and hole densities per unit area $w_{e,h}$ in QW [12, 17]. The energy levels of the QDWELL structure are shown in **Figure 4**.

For the moderate bias currents and comparatively slow processes, the dynamics of the ES-GS transitions can be adiabatically eliminated [12]. Then, the LS rate equations have the form [12, 17]:

$$\begin{aligned}\frac{\partial \rho_{e,h}}{\partial t} &= -W_{ind}A\left(\rho_e+\rho_h-1\right)\left(n_{ph,p}+n_{ph,s}\right)-R_{sp}\left(\rho_e,\rho_h\right)\\ &+S^{in}_{e,h}(w_e,w_h)\left(1-\rho_{e,h}\right)-S^{out}_{e,h}(w_e,w_h)\rho_{e,h}\end{aligned} \tag{13}$$

$$\frac{\partial w_{e,h}}{\partial t}=\frac{J}{e}-2N_{QD}\left[S^{in}_{e,h}(w_e,w_h)\left(1-\rho_{e,h}\right)-S^{out}_{e,h}(w_e,w_h)\rho_{e,h}\right]-\tilde{R}_{sp} \tag{14}$$

where W_{ind} is the Einstein coefficient for the induced emission, A is the in-plane area of QW, N_{QD} is the total QD density per unit area in all QW layers, $S^{in}_{e,h}(w_e,w_h)$, $S^{out}_{e,h}(w_e,w_h)$ are the strongly nonlinear electron and hole scattering rates for the scattering in and out of QD, respectively, $R_{sp}\left(\rho_e,\rho_h\right)=W_{sp}\rho_e\rho_h$, $\tilde{R}_{sp}$ are the spontaneous emission rates in QD and QW, respectively, W_{sp} is the Einstein coefficient for the spontaneous emission. The complicated analytical expressions of $S^{in}_{e,h}(w_e,w_h)$, $S^{out}_{e,h}(w_e,w_h)$ can be found in Ref. [17]. The carrier lifetimes $\tau_{e,h}$ determined by the Coulomb scattering between QD and QW are defined by these

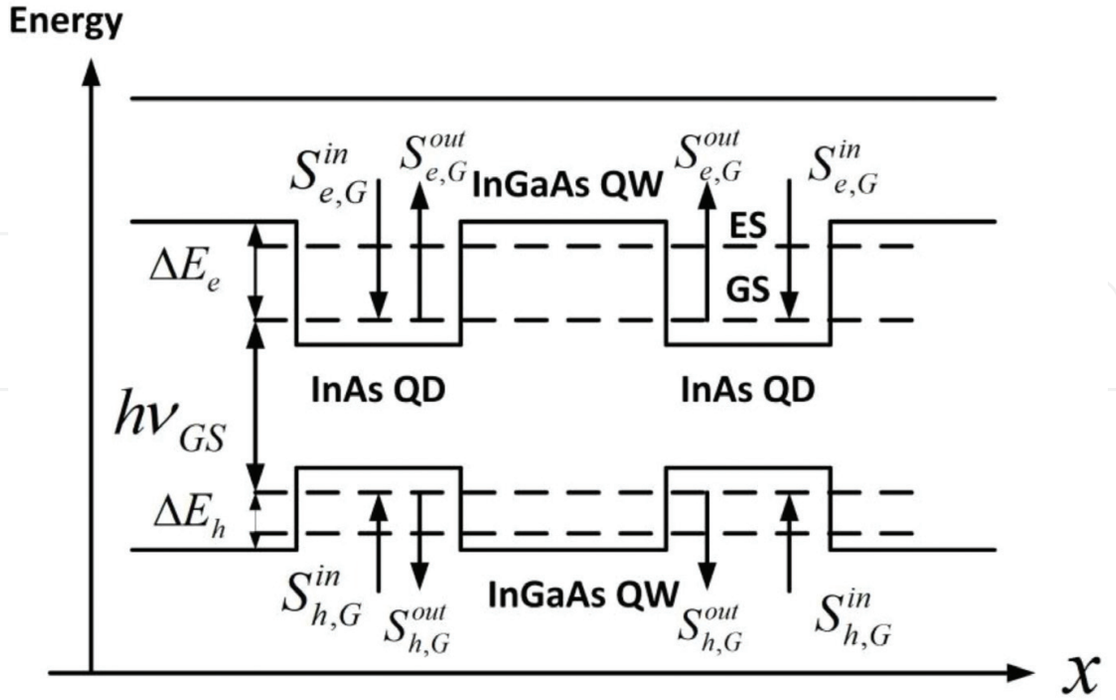

Figure 4. Energy diagram of the QDWELL structure. $\Delta E_{e,h}$ determines the position of the electron and hole GS in QD.

scattering rates as follows [17]: $\tau_e = \left(S_e^{in} + S_e^{out}\right)^{-1}$ and $\tau_h = \left(S_h^{in} + S_h^{out}\right)^{-1}$. Comparison of Eqs. (1), (2) and (13), (14) clearly shows that the QDWELL SOA dynamics is much more complicated than the dynamics of the ordinary QD-SOA. In the case of the QDWELL lasers and SOA, there exist different timescales for electrons and holes in QD and QW reservoir, and for this reason, the carrier dynamics is desynchronized limiting the QDWELL SOA operation rate [12, 38]. The strong optical injection can synchronize the QDWELL laser carrier dynamics in QDWELL lasers and improve their performance [18]. Similarly, in the case of the XGM in the QDWELL SOA, the pumping and signal optical waves play a role of the optical injection according to Eq. (13) and synchronize the carrier dynamics improving QDWELL SOA performance [20–22].

The equations for the pumping and signal wave photon density per unit area $n_{ph,p,s}$ and phases $\Phi_{p,s}$ have the form [20–22, 31]:

$$\frac{\partial n_{ph,p,s}(z,\tau)}{\partial z} = \left(g_{\mathrm{mod}p,s} - \alpha_{\mathrm{int}}\right) n_{ph,p,s}(z,\tau) \tag{15}$$

$$\frac{\partial \Phi_{p,s}}{\partial z} = -\frac{\alpha}{2} g_{\mathrm{mod}p,s} \tag{16}$$

The photon density per unit area $n_{ph,p,s}$ and the photon density $S_{p,s}$ per unit volume are related as follows: $S_{p,s} = \partial n_{ph,p,s}/\partial z$, and $n_{ph,p,s}(0,\tau) = S_{p,s}/\left(g_{\mathrm{mod}p,s} - 2\kappa\right)$ [20]. The QDWELL SOA modal gain $g_{\mathrm{mod}p,s}$ has the form [20]:

$$g_{\mathrm{mod}p,s}(\omega_0) = \frac{2\Gamma N_{QD}}{a}\int d\omega F(\omega)\sigma(\omega_0)\left(\rho_e + \rho_h - 1\right) \tag{17}$$

where $\Gamma = a_L h_{QW}/h_w$ is the confinement factor, a_L is the number of QW layers, $h_{QW} \approx a$ is the height of the QW layer with QD, and h_w is the height of the waveguide. The term $\left(\rho_e + \rho_h - 1\right)$ in Eqs. (13) and (17) describes the electron and hole population inversion in the two-level system of QD. Comparison of Eqs. (13), (15) and (17) shows that the population inversion $\left(\rho_e + \rho_h - 1\right) > 0$ is the necessary condition of the amplification in the QDWELL SOA. Similarly to the previous case of the QD-SOA, we evaluate the spatially averaged over the QDWELL SOA length L photon density per unit area $n_{php,s}(\tau)$ [20]:

$$n_{php,s}(\tau) = \frac{1}{L}\left(n_{php,s}(\tau)\right)_{in}\int_0^L dz\,\exp\left[\int_0^z \left(g_{\mathrm{mod}p,s} - \alpha_{\mathrm{int}}\right)dz'\right] \tag{18}$$

The phases $\Phi_{p,s}$ and the chirp $\Delta\nu_{chirp}^{p,s}$ are given by [20]:

$$\Phi_{p,s} = -\frac{\alpha}{2}\int_0^L g_{\mathrm{mod}p,s}dz;\ \Delta\nu_{chirp}^{p,s} = -\frac{1}{2\pi}\frac{\partial\Phi_{p,s}}{\partial t} \tag{19}$$

The relation between the pumping and signal wave optical power $P_{opt,p,s}(z,\tau)$ and instantaneous pumping and signal photon densities per unit area $n_{ph,p,s}$ can be obtained by using the expressions of $S_{p,s}$. It has the form [20]:

$$\frac{\partial n_{ph,p,s}}{\partial z} = \frac{P_{opt,p,s}(z,\tau)\sqrt{\varepsilon_r}}{2\hbar\omega c A_W} \tag{20}$$

where A_W is the optical waveguide cross-section area.

We solved numerically the system of Eqs. (13)–(16) for the typical values of the material parameters $W_{sp} = 0.7\ ns^{-1}$, $W_{ind} = 0.11\ \mu s^{-1}$, $L = 1\ mm$, $\alpha_{\mathrm{int}} = 12.56\ cm^{-1}$, $A = 4\times10^{-5}\ cm^2$, the bias current density corresponding to the transparency $J_0 = 6.72\times10^5\ Am^{-2}$, $a_L = 15$, $N_{QD} = 10^{11}\ cm^{-2}$, the central pumping and signal wavelengths are $\lambda_p = 1.25\ \mu m$ and $\lambda_s = 1.35\ \mu m$, respectively [17]. In our case, the detuning between the pumping and signal waves $\hbar\left(\omega_p - \omega_s\right) \approx 73.5\ meV > \hbar\gamma_{in\mathrm{hom}}, \hbar\gamma_{\mathrm{hom}}$, and we have taken into account the modal gain inhomogeneous broadening according to Eqs. (17) and (7)–(9). LEF has been chosen to be $\alpha = 10$, which is feasible for QD-SOA [2].

We evaluated the QDWELL SOA gain for $\lambda_s = 1.35\ \mu m$ and for the optical pumping power $P_p = 2\ mW, 5\ mW, 10\ mW$ [20]. The numerical simulation results show that the gain magnitude reaches the level of 20 dB and then decreases with the further increase of the pumping power due to XGM and gain saturation. The QDWELL SOA bandwidth is strongly enhanced due to the fast stimulated transitions in QD caused by the strong optical pumping. The bias

current density slightly influences the gain because of the weak connection between the QW carrier reservoir and QD in the XGM process.

Consider now the synchronization of the carrier dynamics and gain recovery process for the super-Gaussian pulse of the signal wave $\sim \exp\left(-t^4/T_0^4\right)$, $T_0 = 20\ ps$ and the bias current density $J = 2J_0$ [20]. For the small pumping power $P_p = 1\mu W \ll P_s = 1\ mW$, the electron and hole dynamics in QD is desynchronized, and the temporal dependences of $\rho_{e,h}$ are essentially different since their dynamics is determined by the different QD carrier-carrier scattering rates $S^{in}_{e,h}(w_e, w_h)$, $S^{out}_{e,h}(w_e, w_h)$. These nonlinear scattering rates strongly depend on the bias current providing the carriers into the QW reservoir. A comparatively large time interval is necessary for the filling of the QD levels from the QW reservoir. The numerical simulation results show that the QW carrier densities are slightly varying with the deviation of about 1% due to the bias current, while the QD carrier occupation probabilities are approximately equal and varying by 10–20% [20]. The situation changes when the pumping and signal powers are equal and strong enough: $P_p = P_s = 1\ mW$. In such a case, GRT is approximately two times smaller than in the weak pumping case. The behavior of the QD electron and hole occupation probabilities $\rho_{e,h}$ is determined by the sign of the right-hand side (RHS) of Eq. (13). In the case of the strong pumping power P_p, the first term in the RHS of Eq. (13) is dominant providing the fast stimulated transitions in QD. The QD carrier dynamics in such a case synchronized due to the strong optical pumping. The population inversion term $\left(\rho_e + \rho_h - 1\right)$ reaches its minimum value due to the fast recombination process, and the the positive definite term $S^{in}_{e,h}(w_e, w_h)\left(1 - \rho_{e,h}\right) > 0$ in the RHS of Eq. (13) becomes dominant. Then, the QD electron and hole occupation probabilities $\rho_{e,h}$ rapidly increase again. The GRT decreases due to the strong optical pumping.

Consider now the QDWELL SOA large signal response for the electrical PRBS signal with the length of $\left(2^{11} - 1\right)$, repetition frequency of 140 Gb/s, a signal wave power $P_s = 1\ mW$, and the bias current density of $2J_0$ [20]. The numerical simulation results show that for the small optical pumping power $P_p = 1\ \mu W$, the QD and QW carrier dynamics is desynchronized and determined by the scattering rates $S^{in}_{e,h}(w_e, w_h)$, $S^{out}_{e,h}(w_e, w_h)$. The QD levels cannot be filled completely by the capture of carriers from the QW reservoir since the scattering rates $S^{in}_{e,h}(w_e, w_h)$, $S^{out}_{e,h}(w_e, w_h)$ are different for electrons and holes, and the corresponding lifetimes $\tau_e = \left(S^{in}_e + S^{out}_e\right)^{-1}$ and $\tau_h = \left(S^{in}_h + S^{out}_h\right)^{-1}$ are large. As a result, QDWELL SOA exhibits the pattern effect. The chirp $\left|\Delta\nu^s_{chirp}\right| \approx 80\ GHz$ is large and asymmetric.

The QW and QD carrier behavior changes drastically in the case of the strong optical pumping $P_p = P_s = 1\ mW$ even at the same bias current density of $2J_0$. The QD carrier dynamics now is synchronized, the QD electron and hole occupation probabilities $\rho_{e,h}$ remain practically constant at the level of $\rho_e = (0.635 - 0.638)$ and $\rho_h = (0.425 - 0.4285)$ while the positive population inversion $\left(\rho_e + \rho_h - 1\right) > 0$ is slightly varying. The QW carrier dynamics is also synchronized, and the relative variations of the QW carrier densities $w_{e,h}$ are about 10^{-4} [20]. The oscillation period is determined by the optically enhanced GRT. The pattern effect vanishes, and the chirp $\left|\Delta\nu^s_{chirp}\right| \approx 5\ GHz$ sharply reduces and becomes symmetric [20].

Consider now the influence of the optical pumping on the XGM and cross-phase modulation (XPM) of the co-propagating pumping and signal optical waves in QDWELL SOA [20–22]. We suppose that these waves have the same polarization corresponding to a maximum value of the gain since the gain in QDWELL SOA has strong polarization dependence [4]. We investigated the XGM in the in QDWELL SOA both in the pulse regime and in the PRBS regime.

In the pulse regime, for the pulse duration of 5 ps, pump wave power $P_p = 0.4\ \mu W$, the signal wave power $P_s = 1\ mW$ and the bias current density $J = 3J_0$ the QD carrier dynamics is synchronized, and the XGM efficiency is high since the pump wave optical power is depleted almost down to zero [21]. For the pulse duration of 3 ps and the signal wave power increase up to $P_s = 10\ mW$, the QW carrier is also synchronized because the fast light stimulated transitions in QD are dominant. The GRT decreases, the XGM efficiency remains high, the fall time of the signal pulse significantly decreases from about 0.05 ns for $P_s = 1\ mW$ to about 0.01 ns for $P_s = 10\ mW$ while the rise and fall time of the weak pumping pulse do not change [21]. The optical injection enhances the QDWELL SOA bandwidth facilitating the ultra-fast pulse propagation, decreases the spectral broadening, and preserves the pulse waveform.

The synchronized dynamics of the QW and QD carriers in the PRBS regime due to the high level of the optical power also provides the efficient XGM and eliminates the pattern effect [21]. The chirp of output signal wave $\left|\Delta\nu^s_{chirp}\right| \leq 2\ GHz$ remains comparatively small and symmetric. The QDWELL SOA performance is high even at the repetition rate of 140 Gb/s for the signal wave power $P_s = 1\ mW$ and a comparatively strong pumping power $P_p = 2\ mW$ [21]. It deteriorates at the extremely high repetition rate of 250 Gb/s because of the slow carrier dynamics. However, even in such a case, the QDWELL SOA performance can be improved by increasing optical pumping power P_p up to 20 mW [21]. However, for such a strong pumping, the XGM efficiency is decreasing since the gain saturates due to the depletion of the QD carriers. The QD levels are not filling rapidly enough from the QW carrier reservoir.

We theoretically investigated the extinction ratio (ER) dependence on the CW pumping power P_p and the detuning between the signal and pumping optical waves for $P_p = 0.01\ mW$ and $0.1\ mW$, signal wave optical power $P_s = 1\ mW$ and the signal wavelength $\lambda_s = 1.35\ \mu m$ [21]. It has been shown that ER reduces with the increase of the CW pumping power P_p and with the increase of the detuning [21].

4. The applications of QD-SOA in optical signal processing

In this section, we discuss the applications of QD-SOA in all-optical generation of UWB impulse radio signals [24, 25], ultra-fast all-optical processor [27, 28] and all-optical memory [29, 30].

4.1. All-optical generation of UWB impulse radio signals based on MZI with QD-SOA

UWB communication systems are characterized by low power consumption, immunity to multipath fading, precise object location, and high data rates [39]. However, they can operate in the frequency range from 3.1 to 10.6 GHz with an effective isotropic radiated power level of less

than -41 dBm/MHz according to the U.S. Federal Communication Commission (FCC) decision [24, 40]. For this reason, UWB wireless systems are limited by short distances of a several tens of meters [40]. In order to increase the area of coverage, the UWB- over-optical-fiber (UROOF) technology had been proposed [24, 39, 40]. UWB-over-fiber technology can be used for radars, wideband wireless personal area networks (WPAN), sensor networks, imaging systems UWB positioning systems, and so on (see [24] and references therein). In particular, impulse-radio (IR) UWB technology is important where the information is carried by a set of narrow electromagnetic pulses with a bandwidth inversely proportional to the pulse width [24]. Carrier-free impulse modulation avoids complicated frequency mixer, intermediate frequency carrier and filter circuits and has better pass-through characteristic due to the base-band transmission [39]. For instance, Gaussian monocycle and doublet pulses, which are the first and second order derivatives of Gaussian pulse, respectively have lower bit error rate better multipath performance and wider bandwidth as compared to other impulse signals [39, 40].

There exist different methods of the optical IR UWB generation [39–44]. Different optically based systems for the generation of the Gaussian IR UWB monocycles and doublets may include an electro-optic phase modulator (EOPM), a single mode fiber (SMF), erbium-doped fiber amplifier (EDFA), SOA, a fiber Bragg grating (FBG), a photodetector (PD), a Sagnac interferometer, photonic microwave filters [39–44]. The shortages of such systems are the necessity of the complicate electronic circuit for the generation of the short electric Gaussian pulses, the use of EOM and long SMF.

We proposed a novel all-optical method of IR UWB pulse generation based on the integrated MZI with QD-SOA inserted into one arm of the integrated MZI [24]. An intensity-dependent signal interference occurs at the output of the MZI with QD-SOA. The proposed UWB IR signal generation process is based on the XGM and XPM processes in QD-SOA, which are characterized by strong optical nonlinearity and high operation rate as it has been mentioned earlier.

The block diagram of the proposed all-optical UWB IR signal consisting of a CW laser, MZI with a QD-SOA as an active element in the upper arm of the MZI, and a pulsed laser is shown in **Figure 5**. A CW signal of a wavelength λ and an optical power P_0 is split into two signals with the equal optical power $P_0/2$ and inserted into the two ports of the integrated MZI. The train of the short Gaussian pulses generated by the pulsed laser is counter-propagating with respect to the CW optical wave. The optical signal in the lower signal of MZI remains CW while the CW signal propagating through the MZI upper arm transforms into the Gaussian pulse at the MZI output due to the XGM and XPM in the QD-SOA. These pulses from the lower and upper arms interfere at the MZI output. The shape of the output pulse is determined by the power-dependent phase difference $\Delta\theta(t) = \theta_1(t) - \theta_2(t)$ where $\theta_{1,2}(t)$ are the phase shifts in the upper and lower MZI arms, respectively. The MZI output optical power P_{out} is given by [24]

$$P_{out}(t) = \frac{P_0}{2}\left[G_1(t) + G_2(t) - 2\sqrt{G_1(t)G_2(t)}\cos\Delta\theta(t)\right] \tag{21}$$

where $G_{1,2}(t)$ are the amplification factors of the upper and lower MZI arms. In our case, the upper arm amplification factor $\exp(g_{sat}L) \le G_1(t) = \exp(gL) \le \exp(g_0L)$ is limited by the QD-SOA saturation gain g_{sat} and the maximum modal gain g_0 for the linear regime. The lower arm amplification factor $G_2 = 1$. We neglect the losses in the proposed system because of the small

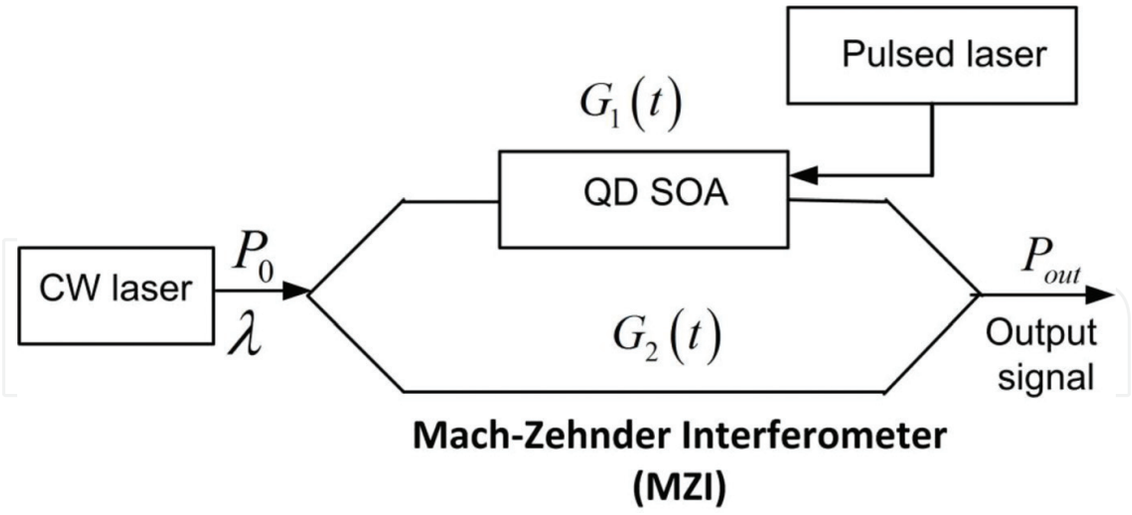

Figure 5. Block diagram of the all-optical UWB IR signal generator based on the MZI with QD-SOA as an active element.

lengths of the integrated elements. The XGM and XPM in QD-SOA are described by Eqs. (1)–(5). The relation between the MZI phase shift $\Delta\theta(t)$ and the upper arm amplification factor $G_1(t)$ has the form $\Delta\theta(t) = -(\alpha/2)\ln G_1(t)$. We solved numerically Eqs. (1)–(5) for the typical values of the QD-SOA material parameters mentioned above, the QD-SOA active region length $L = 2\ mm$, its width $W = 10\ \mu m$, confinement factor $\Gamma = 3 \times 10^{-2}$, the maximum QD-SOA gain $g_{\max} = 11.5\ cm^{-1}$, and the QD-SOA losses $\alpha_{\text{int}} = 3\ cm^{-1}$ [24]. The simulation results show that at the high Gaussian pulse power levels, QD-SOA passes to the saturation regime accompanied by the decrease of the XPM phase shift $\Delta\theta(t)$ and the upper arm amplification factor $G_1(t)$ to their minimum values. In such a case, the MZI output signal power P_{out} also has its minimum value due to the maximum value of the oscillating term in Eq. (21). Then, the XPM process is dominant, and the Gaussian doublet occurs at the MZI output [24]. In the opposite case of the weak Gaussian pulse, QD-SOA operates in the linear regime, and the Gaussian pulse remains unchanged [24]. The simulation results for the temporal dependence of the output signal power, optical signal power in the MZI upper and lower arms, and the MZI phase difference for the pulse power $P_p = 0.5\ mW$ and the CW power $P_{CW} = 0.005\ mW$ are presented in **Figure 6**. Different input power levels provide different contributions of the XGM and XPM processes in QD-SOA, which results in the different shapes of the MZI output pulses. Actually, the shape of the signal and its spectrum can be tailor-made [24].

The spectrum of the simulated UWB IR signal exhibits the filtering features of the proposed generator [24]. Indeed, for the Gaussian pulses duration $\sim 10^{-11}\ s$, a rise time and a fall time of the pulse propagating through the QD-SOA are limited by the fast transition time $\tau_{12} \sim 1\ ps$ between GS and ES.

4.2. Ultrafast all-optical processor based on QD-SOA

The major application areas of SOA-based MZI are all-optical logic gates, optical WC, and optical regenerators. The latter devices provide the so-called 3R regeneration [3], that is,

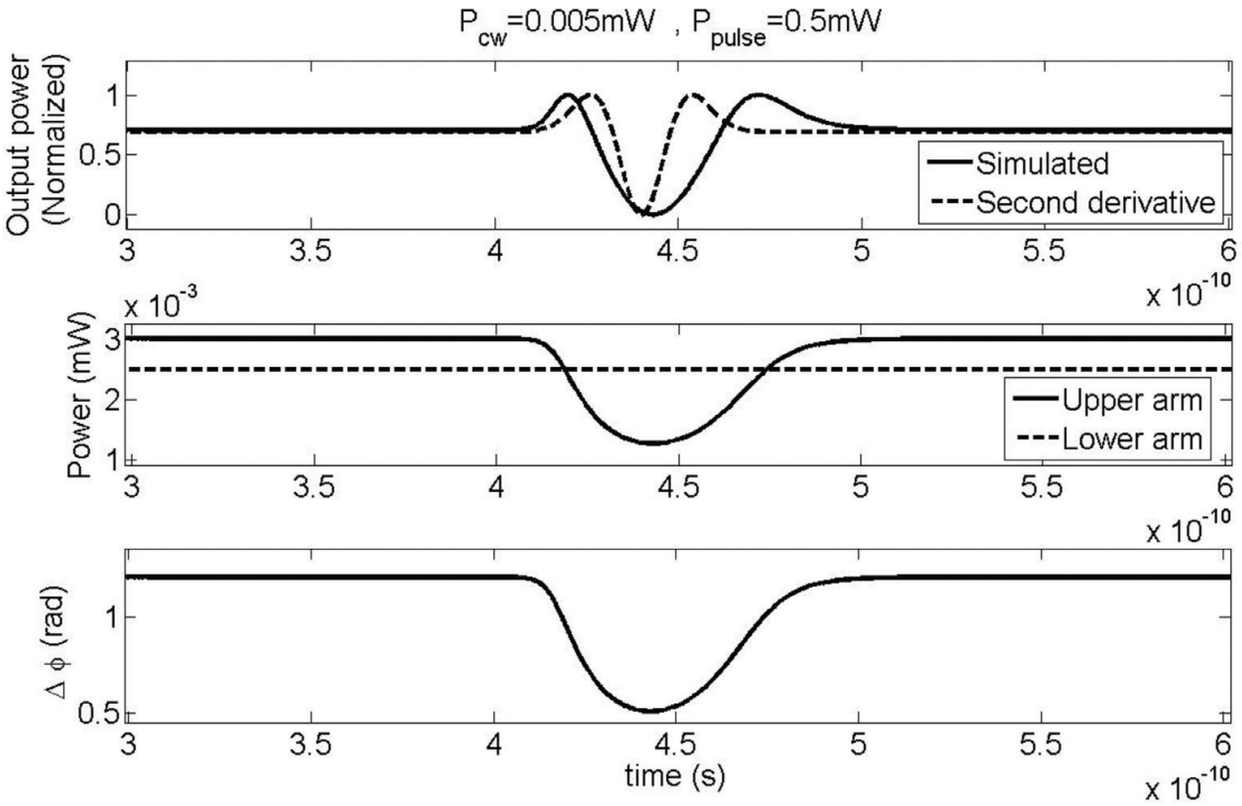

Figure 6. The temporal dependence: Gaussian doublet (solid line) and the second derivative of the Gaussian pulse (dashed line) for $P_p = 0.5\ mW$ and $P_{CW} = 0.005\ mW$ (the upper box); the optical signal power in the MZI upper arm (solid line) and the lower arm (dashed line) (intermediate box); the phase difference (lower box).

re-amplification, re-shaping, and re-timing which are necessary for the elimination of the noise, crosstalk and nonlinear distortions and for the transmission of the good quality signals over sufficiently large distances in all-optical networks (see [27, 28] and references therein).

We proposed a theoretical model of an ultrafast all-optical signal processor based on MZI containing QD-SOA in each arm (QD-SOA-MZI) where XOR logic operation, wavelength conversion, and 3R signal regeneration can be realized simultaneously by AO-XOR logic gates for the bit rates up to 100 Gb/s for the bias current $I \approx 30\ mA$ and 200 Gb/s for the bias current $I \approx 50\ mA$ [27].

The block diagram of AO-XOR logic gate based on the QD-SOA-MZI is shown in **Figure 7**.

The theoretical analysis of the proposed processor is based on the QD-SOA dynamics described by Eqs. (1)–(5) and the expression for the MZI output power (21). However, this time, QD-SOA are situated in both arms of the MZI, and the QD-SOA amplification factors $G_{1,2}(t)$ have the form $G_{1,2}(t) = \exp\left(g_{1,2}L_{1,2}\right)$ where $g_{1,2}; L_{1,2}$ are the first and second QD-SOA gains and active region lengths, respectively. When the control signal A and/or B are fed into the two QD-SOA, they modulate the SOA gains and also phase of the co-propagating CW signal due to LEF α according to Eq. (5). The phase shift at the QD-SOA-MZI has the form [27]:

$$\Delta\theta(t) = -(\alpha/2)\ln[G_1(t)/G_2(t)] \tag{22}$$

For the typical values of LEF $\alpha = (5-7)$, gain $g_{1,2} = 11.5\ cm^{-1}$ and $L_{1,2} = 1500\ \mu m$ the phase shift of about π can be achieved.

We start with the operation of the logic gate based on the QD-SOA-MZI, which consists of a symmetrical MZI with one QD-SOA in each arm [27, 28]. Two optical control beams A and B at the same wavelength λ are fed into the ports A and B of QD-SOA-MZI separately. A third signal representing a clock stream of CW series of unit pulses is split into two equal parts and injected in two QD-SOA. Two cases of the detuning between the signals A, B and the clock stream may occur. If the detuning is less than the QD homogeneous broadening, then the ultrafast operation can be realized. If the detuning is large and compared to the QD inhomogeneous broadening XGM in DQ SOA is also possible due to the QD interaction through WL for the comparatively low bit rates up to 10 Gb/s [11]. Such a case is discussed in subsection 2.3.

Suppose that the data stream at the input of the QD-SOA-MZI is absent: $A = B = 0$. In such a case, the phase difference of the signal propagating through both arms of QD-SOA-MZI is π, and the output signal is "0" because of the destructive interference [27]. Let now $A = 1, B = 0$. Then, the signal propagating through the upper arm and interacting with the data stream A acquires the additional phase determined by XPM between the signal and A while the phase of the signal propagating through the lower arm of the QD-SOA-MZI does not change. As a result, the output signal is "1" [27]. Evidently, the same output corresponds to the input $A = 0, B = 1$. Finally, in the case when $A = 1, B = 1$ the phase changes of the signal in both arms of the QD-SOA-MZI are equal, and the output signal is "0" [27].

Consider now the wavelength conversion in the proposed processor. An ideal WC must be characterized by the following properties: transparency to different bit rates and signal formats, fast setup of the output wavelength, the possibility of conversion to shorter and longer wavelengths, moderate input power levels, the possibility for no conversion regime, insensitivity to

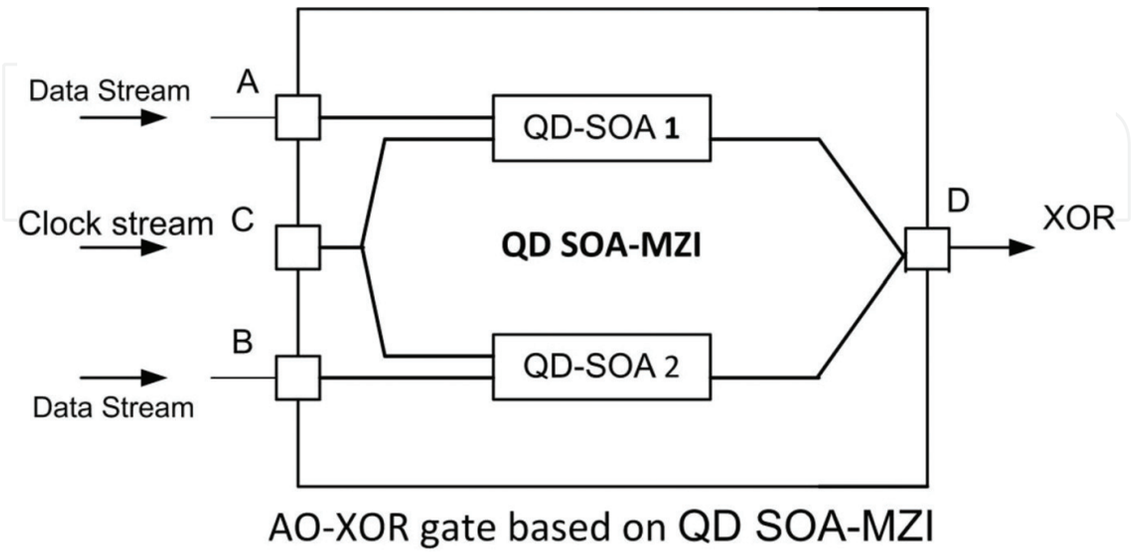

Figure 7. The block diagram of the AO-XOR logic gate based on QD-SOA-MZI.

http://dx.doi.org/10.5772/intechopen.74655

the input signal polarization, the output signal with low chirp, high ER and large signal-to-noise ratio (SNR), and simple implementation [45]. SOA is a promising candidate for applications in WC because it possesses these characteristics.

WC performance can be substantially improved by replacing the bulk SOA with QD-SOA due to its specific features discussed in Section 2: the pattern-free high-speed wavelength conversion of optical signals by XGM, a low threshold current density, a high material gain, high saturation power, broad gain bandwidth, and a weak temperature dependence as compared to bulk and MQW SOA [9–11]. In the proposed ultrafast all-optical processor, the advantages of the QD-SOA as a nonlinear component and of the MZI as a system with the controlled output signal [27, 28]. Consider the situation where one of the inputs signals A or B is absent. In such a case, CW signal with the required output wavelength is split asymmetrically between the QD-SOA-MZI arms and interferes at the QD-SOA-MZI constructively or destructively with the intensity modulated input signal at another wavelength. The interference result depends on the phase difference between the two QD-SOA-MZI arms output, which is actually determined by the corresponding QD-SOA. The QD-SOA-MZI operates as an amplifier of the propagating signal. The operation with the output "1" can be defined as a wavelength conversion caused by XGM between the input signal A or B and the clock stream signal [27, 28]. The $(10-40)\ Gb/s$ pattern-effect-free wavelength conversion by XGM at the wavelength $\lambda = 1.3\ \mu m$ using QD-SOA with InGaAs/GaAs self-assembled QD had been demonstrated experimentally [7].

The deterioration of the ultrafast all-optical processor with the bit rate increase is shown in **Figures 8** and **9**. For the bias current $I = 30\ mA$ and the bit rate of 100 Gb/s, the patterning effect is moderate, and the eye in the eye diagram is open (**Figure 8**). For the bit rate of 200 Gb/s at the same bias current, the patterning effect is strongly pronounced, and the eye is closed (**Figure 9**).

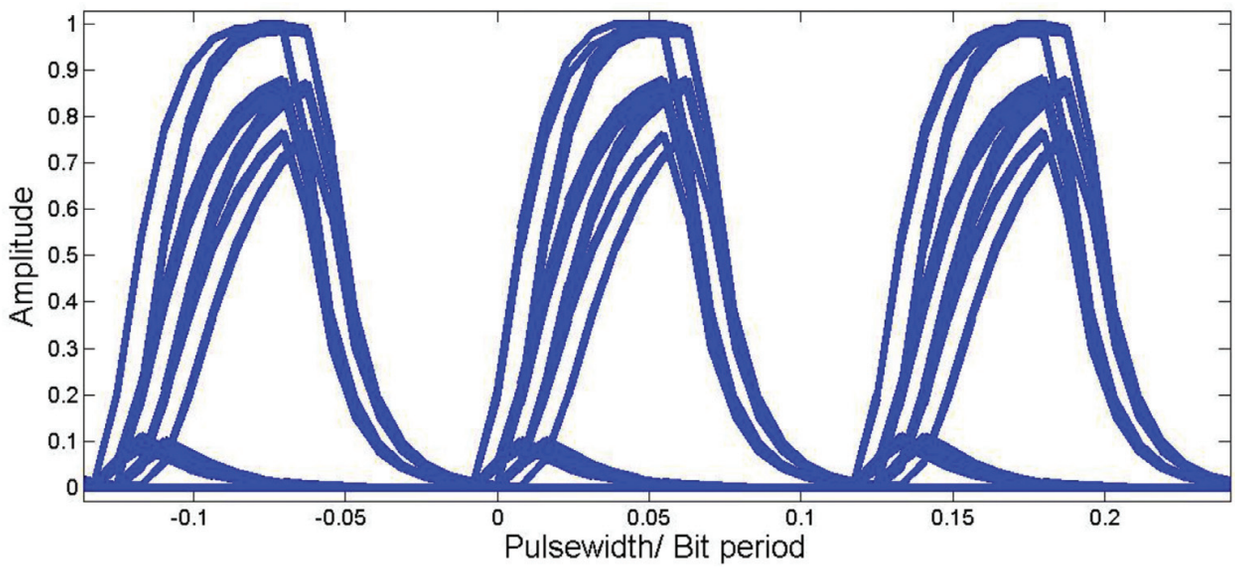

Figure 8. The eye diagram for the bit rate 100 Gb/s, the bias current $I = 30\ mA$.

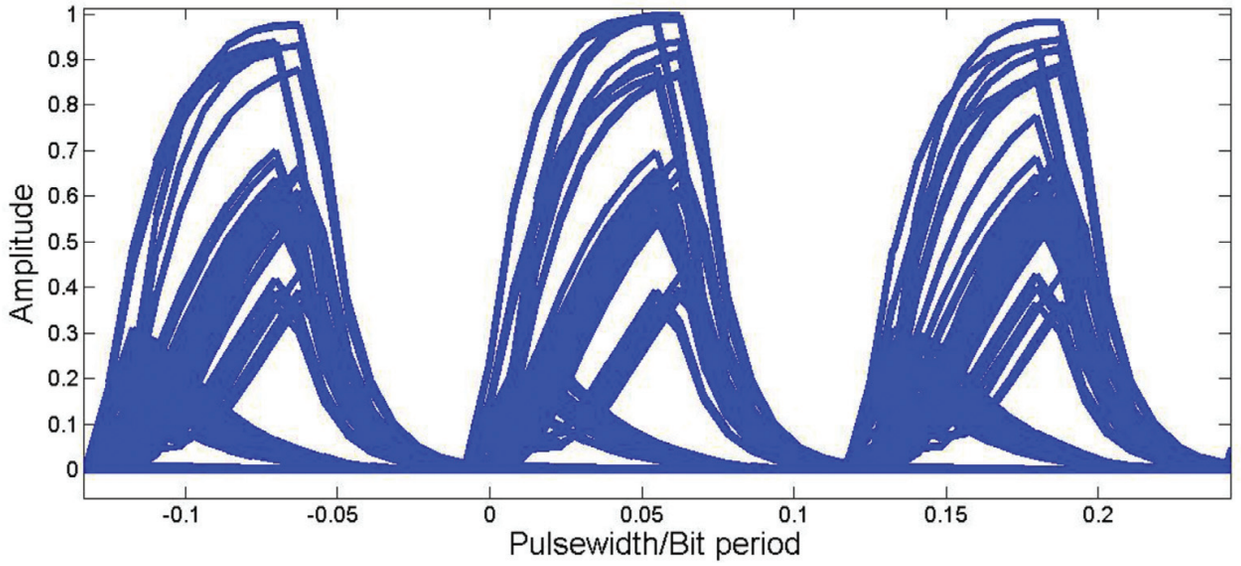

Figure 9. The eye diagram for the bit rate 200 Gb/s, the bias current $I = 30\ mA$.

The proposed ultrafast all-optical processor can solve three problems of the short pulse 3R regeneration mentioned above [27, 28]. The efficient pattern-effect-free signal re-amplification can be realized in each of the QD-SOA-MZI by the corresponding QD-SOA. The wavelength conversion based on all-optical logic gate discussed above can provide the reshaping since only the data signals can close the gate, while the comparatively weak noise cannot close the gate. The re-timing in the QD-SOA-MZI-based processor is provided by the optical clock stream, which is also necessary for the re-shaping. If the CW input signal is replaced with the optical clock stream, the 3R regeneration can be carried out simultaneously with the logic operations [27, 28].

4.3. Ultrafast all-optical memory based on QD-SOA

Optically assisted signal processing combines optical and electronic components [46]. For instance, optical components characterized by high operation rate can carry out some functions very fast, while the electronic components can realize the complex computations using buffers and memory [46]. In optical networks, the bandwidth mismatch between optical transmission and electronic routers requires a different optical signal processing and the study of the optical packet switching (OPS) [47]. The packet switching is used when it is necessary to select a packet of tens or hundreds of bits from a bit stream [48]. The flip-flop memory is an essential component of the packet switch in OPS networks, which is necessary for avoiding the packet collisions during packet routing [48, 49]. Usually, this memory consists of two coupled lasers switching the output signal between the wavelengths λ_1 and λ_2 [48]. We proposed a novel architecture of the all-optical memory loop based on the ultra-fast all-optical signal processor discussed in subsection 4.2 [29, 30]. The block diagram of the all-optical memory loop is shown in **Figure 10**.

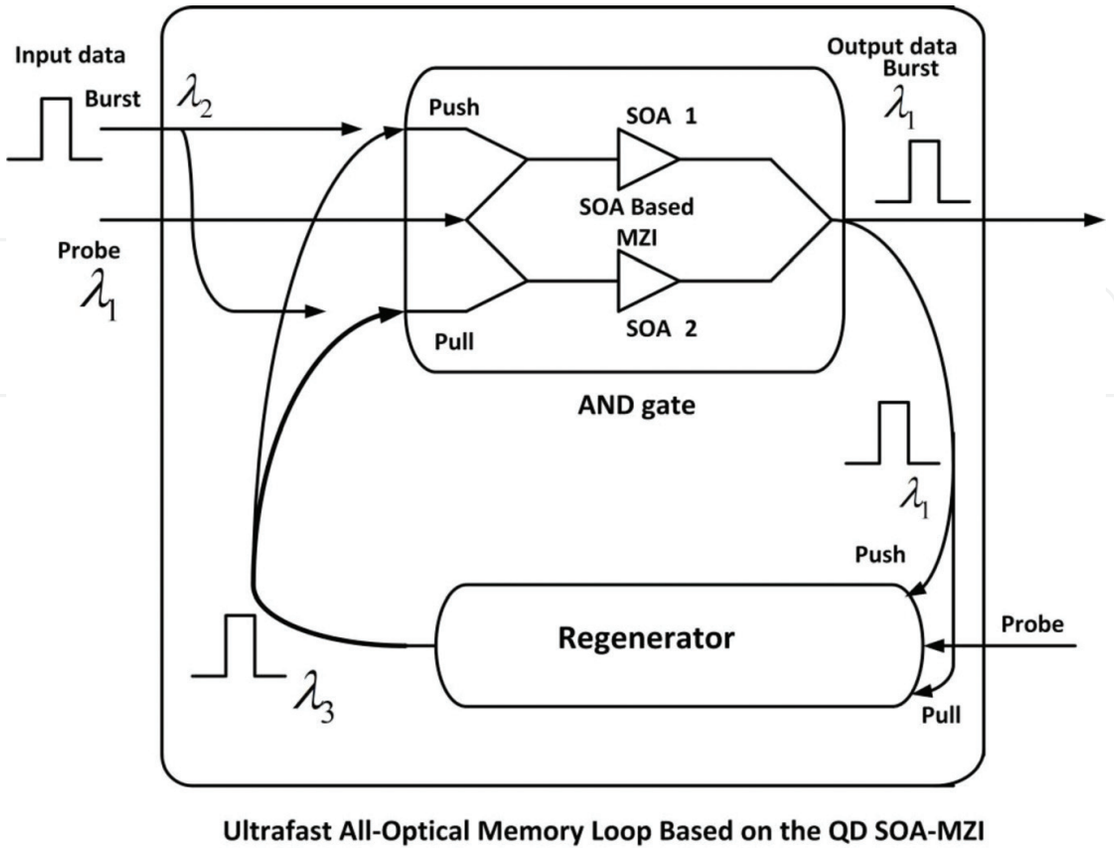

Figure 10. The block diagram of the ultrafast all-optical memory based on the QD-SOA-MZI.

The novel all-optical memory loop is characterized by the following advantages: (1) it includes only one QD-SOA-MZI reducing the complexity of the electronic synchronization scheme; (2) it can operate at the high bit rates up to 100 Gb/s due to fast GRT of QD-SOA discussed in subsection 2.2; (3) a regenerator is included into the loop for the optical fiber loss compensation and increasing of the loop length [28, 29]. The regenerator can be also based on SOA as it was mentioned above.

The QD-SOA dynamics and the ultra-fast all-optical processor operation principle have been discussed in detail in Section 2 and subsection 4.2, respectively. The theoretical model of the proposed all-optical memory loop is based on the QD-SOA carrier rate Eqs. (1)–(3), the average pump and signal wave photon densities $S_{p,s}(\tau)$ expression (10), the pump and signal wave phase $\theta_{p,s}$ expression (11), the modal gain $g_{p,s}$ expression (6), and the MZI output power P_{out} and phase difference $\Delta\theta$ expressions (21), (22), respectively. The phase difference $\Delta\theta$ at the output of the QD-SOA-MZI is defined by the optical signal power difference in the upper and lower arms of the QD-SOA-MZI. Typically, 80% and 20% of the input signal power were injected through the coupler into the upper and lower arms of the QD-SOA-MZI, respectively. Consequently, the dynamic processes in QD-SOA placed into the upper and lower arms of MZI are determined by different carrier relaxation time and GRT as it was mentioned in Section 2.

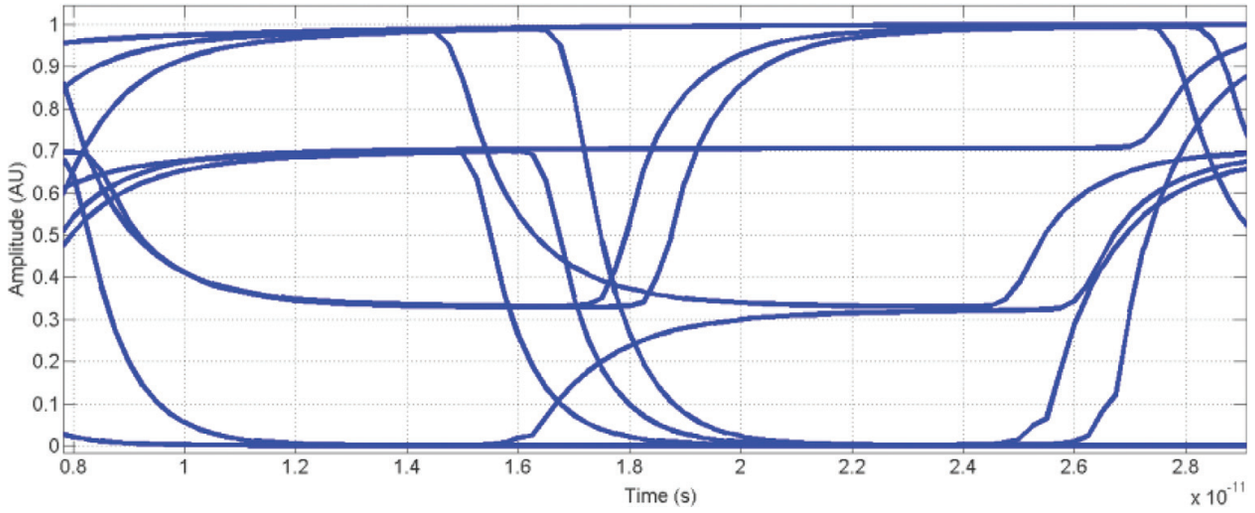

Figure 11. The eye diagram for the 4 PAM modulation format, a bit rate of 100 Gb/s; the signal is after one round in the all-optical memory loop.

We solved numerically Eqs. (1)–(3), (10), (11), (21), and (22) for the typical values of the material parameters presented in Section 2 in two cases: (1) the on–off keying (OOK) modulation format, the loop length $L_{loop} = 2\ km$, the bit rate 50 Gb/s and the quality factor at the input $Q = 15.8932$; (2) the pulse modulation 4 (4-PAM) format, the loop length $L_{loop} = 1\ km$, the bit rates 50 Gb/s and 100 Gb/s [28, 29]. In the case of the OOK modulation format, the numerical simulation results show that after four rounds in the loop the signal quality factor Q decreases by approximately 18% to 13.3156, and the patterning effect is slightly pronounced [28, 29]. In the case of the 4-PAM format, the patterning effect is negligible after two rounds in the loop for the bit rate of 50 Gb/s and it is slightly pronounced for the bit rate of 100 Gb/s [28, 29]. Hence, the performance of the QD-SOA-based all-optical memory does not deteriorate substantially up to the bit rate of 100 Gb/s.

For instance, the eye diagram for the 4 PAM modulation format and a bit rate of 100 Gb/s after 1 round in the all-optical memory loop is shown in **Figure 11**.

The numerical estimations show that for the loop length $L_{loop} = 1\ km$, the light velocity in the optical fiber $v \approx 2 \times 10^8\ m/s$ and the bit rates of 50 Gb/s and 100 Gb/s the all-optical storage values are of $0.25Mb$ and $0.5Mb$, and the storage times are $5\mu s$ and $10\mu s$, respectively [28, 29].

5. Conclusions

We studied theoretically the dynamics of QD-SOA. We solved numerically the QD-SOA carrier rate equations simultaneously with the truncated equations for the light wave photon density and phase. We have shown that the injection of the additional light wave drastically changes the QD-SOA dynamics. As a result, GRT may be strongly reduced by using the short Gaussian pulses and strong additional light wave. The lower GRT limit is defined by the QD-SOA fastest transition between ES and GS with the transition time $\tau_{21} = 0.16\ ps$. We investigated

theoretically the specific features of XGM in QD-SOA. We have shown that the patterning effect manifests for the bit rates of about 10 Gb/s, but it can be diminished by increase of the bias current. However, at the higher bit rates of about 40 Gb/s, the bias current does not influence the patterning effect. The interaction between the nonresonant QD groups for the signal and pumping light waves with the detuning larger than the QD homogeneous broadening is possible for the large bias currents and fast pulses with the duration of nanoseconds and several dozen picoseconds. In such a case, QD can interact through WL due to the sufficiently fast relaxation carrier from WL to QD. QD-SOA have the lowest bias current, the highest operation bit rate, and the large gain bandwidth as compared to the bulk and MQW SOA. For this reason, they are the promising candidates for the all-optical signal processing.

The novel generation of QD lasers and SOA is based on the QDWELL structures where the self-assembled QD is imbedded into QW layers. The QW layers play a role of the reservoir for the 2D carrier gas instead of WL with the continuous carrier energy in ordinary QD-SOA. The complicated QDWELL laser and SOA dynamics are described by the system of LS rate equations for electrons and holes in QD and QW. The QDWELL laser and SOA performance are limited by the strongly desynchronized dynamics of electrons and holes in QD and QW. The different relaxation times of the electrons and holes in QW and QD are determined by the strongly nonlinear electron and hole scattering rates in and out of QD.

We solved numerically the modified LS rate equations and the truncated equations for the pumping and signal waves in the QDWELL SOA for the pulse regime and the large PRBS signal. We have shown that the strong optical injection with the power $(1-10)\ mW$ synchronizes the carrier dynamics in QDWELL SOA because the fast light stimulated transitions become dominant. The bias current remains comparatively low preventing the device heating. The propagation of the signal and CW pumping waves gives rise to the XGM. In such a case, the pumping wave in QDWELL SOA plays a role of the synchronizing optical injection. As a result, the QDWELL SOA performance significantly improves, the fast gain recovery occurs, the patterning effect vanishes, and the operation rate increases up to 140 Gb/s.

The QD-SOA can be successfully used in the all-optical signal processing due to their strong nonlinearity, high operation rate, and low bias current. We proposed a novel all-optical method of the UWB IR signal generation based on the integrated MZI with QD-SOA in each arm as a nonlinear element. The proposed method does not need SMF, EOPM, and FBG reducing complexity and cost of the UWB IR generator. The UWB IR signal generated by the QD-SOA-based MZI has a form of the Gaussian doublet.

We proposed a theoretical model of the ultrafast all-optical signal processor also based on QD-SOA-MZI structure. We have shown theoretically that such a processor may realize logic gate XOR operation, wavelength conversion, and 3R regeneration of the moderately distorted optical signals. The operation of the processor is based on the XGM and XPM in QD-SOA in both arms of the MZI. The processor limiting bit rate depends on the bias current I and may reach 200 Gb/s for $I = 50\ mA$.

We proposed a novel architecture of the ultra-fast all-optical memory based on MZI with two QD-SOAs. The numerical simulation results for the OOK and 4 PAM modulation format show

that the proposed memory is characterized by high operation rate up to 100 Gb/s due to the QD-SOA fast dynamics and in particular rapid gain recovery process. Evaluations show that for the 4 PAM modulation format, $l = 1km$ light velocity in the optical fiber $v \approx 2 \times 10^8\ m/s$ and typical values of the bit rate of 50 Gb/s and 100 Gb/s the memory storage values are 0.25 Mb and 0.5 Mb, respectively. The corresponding storage times are 5 μs and 10 μs, respectively.

Author details

Yossef Ben Ezra and Boris I. Lembrikov*

*Address all correspondence to: borisle@hit.ac.il

Department of Electrical Engineering and Electronics, Holon Institute of Technology (HIT), Holon, Israel

References

[1] Akiyama T, Sugawara M, Arakawa Y. Quantum-dot semiconductor optical amplifiers. Proceedings of the IEEE. 2007;**95**:1757-1766. DOI: 10.1109/JPROC2007.900899

[2] Rafailov EU, Cataluna MA, Avrutin EA. Ultrafast Lasers Based on Quantum Dot Structures. 1st ed. Wiley-VCH: Weinheim; 2011. p. 261. ISBN: 978-3-527-40928-0

[3] Sugawara M, Akiyama T, Hatori N, Nakata Y, Ebe H, Ishikawa H. Quantum-dot semiconductor optical amplifiers for high-bit-rate signal processing up to 160 Gbs^{-1} and a new scheme of 3R regenarators. Measurement Science and Technology. 2002;**13**:1683-1691. DOI: 10.1088/0957-0233/13/11/304

[4] Bakonyi Z, Onishchukov G, Lester LF, Gray AL, Newell TC, Tünnermann A. High-gain quantum-dot semiconductor optical amplifier for 1300 nm. IEEE Journal of Quantum Electronics. 2003;**39**:1409-1414. DOI: 10.1109/JQE.2003.818306

[5] Qasaimeh O. Optical gain and saturation characteristics of quantum-dot semiconductor optical amplifiers. IEEE Journal of Quantum Electronics. 2003;**39**:793-798. DOI: 10.1109/JQE.2003.810770

[6] Harrison P. Quantum Wells, Wires and Dots. 2nd ed. UK: Wiley; 2005. p. 508. ISBN: 978-0-470-01080-8 (PB)

[7] Sugawara M, Ebe H, Hatori N, Isida M, Arakawa Y, Akiyama T, Otsubo K, Nakata Y. Theory of optical signal amplification and processing by quantum-dot optical amplifiers. Physical Review B. 2004;**69**:235332-1-235332-39. DOI: 10.1103/PhysRevB.69.235332

[8] Qasaimeh O. Characteristics of cross-gain (XG) wavelength conversion in quantum-dot semiconductor optical amplifiers. IEEE Photonics Technology Letters. 2004;**16**:542-544. DOI: 10.1109/LPT.2003.821047

[9] Ben-Ezra Y, Haridim M, Lembrikov BI. Theoretical analysis of gain-recovery time and chirp in QD-SOA. IEEE Photonics Technology Letters. 2005;**17**:1803-1805. DOI: 10.1109/LPT.2005.853030

[10] Ben-Ezra Y, Haridim M, Lembrikov BI. Acceleration of gain recovery and dynamics of electrons in QD-SOA. IEEE Journal of Quantum Electronics. 2005;**41**:1268-1273. DOI: 10.1109/JQE.2005.854131

[11] Ben-Ezra Y, Haridim M, Lembrikov BI. Specific features of XGM in QD-SOA. IEEE Journal of Quantum Electronics. 2007;**43**:730-737. DOI: 10.1109/JQE.2007.901587

[12] Lüdge K. Modeling quantum-dot-based devices. In: Lüdge K, editor. Nonlinear Laser Dynamics. Weinheim, Germany: Wiley; 2012. pp. 3-33. ISBN: 978-3-527-41100-9

[13] Meuer C, Kim J, Laemmlin M, et al. High-speed small-signal cross-gain modulation in quantum-dot semiconductor optical amplifiers at 1.3 μm. IEEE Journal of Selected Topics in Quantum Electronics. 2009;**15**:749-756. DOI: 10.1109/JSTQE.2009.2012395

[14] Kim J, Laemmlin M, Meuer C, Bimberg D, Eisenstein G. Theoretical and experimental study of high-speed small-signal cross-gain modulation of quantum-dot semiconductor optical amplifiers. IEEE Journal of Quantum Electronics. 2009;**45**:240-248. DOI: 10.1109/JQE.2008.2010881

[15] Wegert M, Majer N, Lüdge K, et al. Nonlinear gain dynamics of quantum dot optical amplifiers. Semiconductor Science Technology. 2011;**26**:1-11. DOI: 10.1088/0268-1242/26/1/014008

[16] Wilkinson S, Lingnau B, Korn J, Schöll E, Lüdge K: Influence of noise on the signal quality of quantum-dot semiconductor optical amplifiers. IEEE Journal of Selected Topics in Quantum Electronics 2013; 19: 1900106-1-1900106-6. DOI: 10.1109/JSTQE.2012.2233464

[17] Pausch J, Otto C, Tylaite E, Majer N, Schöll E, Lüdge K. Optically injected quantum dot lasers: Impact of nonlinear carrier lifetimes on frequency-locking dynamics. New Journal of Physics. 2012;**14**:1-20. DOI: 10.1088/1367-2630/14/053018

[18] Ben-Ezra Y, Lembrikov BI. Synchronized carrier dynamics in quantum dot-in-a-well (QDWELL) laser under an optical injection. IEEE Journal of Selected Topics in Quantum Electronics. 2013;**19**:1901508-1-1901508-8. DOI: 10.1109/JSTQE.2013.2246770

[19] Ben-Ezra Y, Lembrikov BI. Quantum dot-in-a-well (QDWELL) laser dynamics under optical injection. Optical and Quantum Electronics. 2014;**46**:1239-1245. DOI: 10.1007/s11082-013-9829-3

[20] Ben-Ezra Y, Lembrikov BI. Semiconductor optical amplifier based on a quantum dot-in-a-well (QDWELL) structure under optical pumping. IEEE Journal of Quantum Electronics. 2014;**50**:340-347. DOI: 10.1109/JQE.2014.2308393

[21] Ben-Ezra Y, Lembrikov BI. Investigation of a cross-gain modulation (XGM) in a semiconductor optical amplifier (SOA) based on a quantum dot-in-a-well (QDWELL) structure. IET Optoelectronics. 2015;**9**:43-51. DOI: 10.1049/iet-opt.2014.0061

[22] Ben-Ezra Y, Lembrikov B. I: Improvement of the quantum dot-in-a-well (QDWELL) laser and amplifier performance under the optical injection. In: Pinho P, editor. Optical Communication Technology. Rijeka, Croatia: InTech; 2017. pp. 75-99. DOI: 10.5772/intechopen.69946

[23] Agrell E, Karlsson M, Chraplyvy AR, et al. Roadmap of optical communications. Journal of Optics. 2016;**18**(063002):1-40. DOI: 10.1088/2040-8978/18/6/063002

[24] Ben-Ezra Y, Haridim M, Lembrikov BI, Ran M. Proposal for all-optical generation of ultra wideband impulse radio signals in Mach-Zehnder interferometer with quantum dot optical amplifier. IEEE Photonics Technology Letters. 2008;**20**:484-486. DOI: 10.1109/LPT.2008.918256

[25] Ben Ezra Y, Lembrikov BI, Ran M, Haridim M. All-optical generation and processing of IR UWB signals. In: Lethien C, editor. Optical Fibre, New Developments. Vucovar, Croatia: InTech; 2009. pp. 425-444. ISBN: 978-953-7619-50-3

[26] Ran M, Ben-Ezra Y, Lembrikov BI. High performance analog optical links based on quantum dot devices for UWB signal transmission. In: Lembrikov BI, editor. Ultra-Wideband. InTech: Croatia; 2010. pp. 75-96. ISBN: 978-953-307-139-8

[27] Ben Ezra Y, Lembrikov BI, Haridim M. Ultra-fast all-optical processor based on quantum dot semiconductor optical amplifiers. IEEE Journal of Quantum Electronics. 2009;**45**:34-41. DOI: 10.1109/JQE.2008.2003497

[28] Ben Ezra Y, Lembrikov BI. New approach to ultra-fast all-optical signal processing based on quantum dot devices. In: Grym J, editor. Semiconductor Technologies. Croatia: InTech; 2010. pp. 419-436. ISBN: 978-953-307-080-3

[29] Ben Ezra Y, Lembrikov BI. All-optical memory based on quantum dot semiconductor optical amplifiers (QD-SOAs) for advanced modulation formats. In: Proceedings of 18th Int'l. Conf. on Transparent Optical Networks (ICTON 2016); July 10–14, 2016; Trento, Italy, Tu.A5.3 1–3. ISBN: 978–1–5090-1466-8

[30] Ben Ezra Y, Lembrikov BI. Ultra-fast all-optical memory based on quantum dot semiconductor optical amplifiers (QD-SOA). In: Roka R, editor. Optical Fiber and Wireless Communications. Rijeka, Croatia: InTech; 2017. pp. 279-293. DOI: 10.5772/intechopen.68527

[31] Uskov AV, Berg WT, Mork J. Theory of pulse-train amplification without patterning effects in quantum-dot semiconductor optical amplifiers. IEEE Journal of Quantum Electronics. 2004;**40**:306-320. DOI: 10.1109/JQE.2003.823032

[32] Qasaimeh O. Novel closed-form model for multiple-state quantum-dot semiconductor optical amplifiers. IEEE Journal of Quantum Electronics. 2008;**44**:652-657. DOI: 10.1109/JQE.2008.922324

[33] Borri P, Langbein W, Hvam JM, Heinrichsdorff F, Mao M-H, Bimberg D. Ultrafast gain dynamics in InAs-InGaAs quantum-dot amplifiers. IEEE Photonics Technology Letters. 2000;**12**:594-596. DOI: S 1041-1135(00)04605-X

[34] Berg WT, Bischoff S, Magnusdottir I, Mork J. Ultrafast gain recovery and modulation limitations in self-assembled quantum-dot devices. IEEE Photonics Technology Letters. 2001;**13**:541-543. DOI: S 1041-1135(01)04546-3

[35] Pleumeekers JL, Kauer M, Dreyer K, et al. Acceleration of gain recovery by optical injection in semiconductor optical amplifiers by optical injection near transparency wavelength. IEEE Photonics Technology Letters. 2002;**14**:12-14. DOI: S 1041-1135(02)00011-3

[36] Connely MJ. Semiconductor Optical Amplifiers. Dordrecht, The Netherlands: Cluver; 2002. p. 169. ISBN: 0-7923-7657-9

[37] Contestabile G, Maruta A, Sekiguchi S, Morito K, Sugawara M, Kitayama K. Cross-gain modulation in quantum-dot SOA at 1550 nm. IEEE Journal of Quantum Electronics. 2010; **46**:1696-1703. DOI: 10.1109/JQE.2010.2060714

[38] Lüdge K, Schöll E. Quantum-dot lasers desynchronized nonlinear dynamics of electrons and holes. IEEE Journal of Quantum Electronics. 2009;**45**:1396-1403. DOI: 10.1109/JQE.2009.2028159

[39] Chen H, Chen M, Wang T, Li M, Xie S. Methods for ultra-wideband pulse generation based on optical cross-polarization modulation. Journal of Lightwave Technology. 2008; **26**:2492-2499. DOI: 10.1109/JLT.2008.927616

[40] Zeng F, Yao J. An approach to ultra-wideband pulse generation and distribution over optical fiber. IEEE Photonics Technology Letters. 2006;**18**:823-825. DOI: 10.1109/LPT.2006.871844

[41] Lin W-P, Chen Y-C. Design of a new optical impulse radio system for ultra-wideband wireless communications. IEEE Journal of Selected Topics in Quantum Electronics. 2006; **12**:882-887. DOI: 10.1109/JSTQE.2006.876613

[42] Li J, Xu K, Fu S, et al. Ultra-wideband pulse generation with flexible pulse shape and polarity control using a Sagnac-interferometer-based intensity modulator. Optics Express. 2007;**15**:18156-18161. ISSN: 1094-4087

[43] Zeng F, Wang Q, Yao J. All-optical UWB impulse generation based on cross-phase modulation and frequency discrimination. Electronics Letters. 2007;**43**:121-122. ISSN: 0013-5194

[44] Zeng F, Yao J. Ultra-wideband impulse radio signal generation using a high-speed electro-optic phase modualtor and a fiber-Bragg-grating–based frequency discriminator. IEEE Photonics Technology Letters. 2006;**18**:2062-2064. DOI: 10.1109/LPT.2006.883310

[45] Ramamurthy B. Swithches, wavelength routers, and wavelength converters. In: Sivalingam KM, Subramaniam S, editors. Optical WDM Networks. Principles and Practice. Boston: Kluwer; 2001. pp. 51-75 0-7923-7825-3

[46] Willner AE, Khaleghi S, Chitgarha MR, Yilmaz OF. All-optical signal processing. Journal of Lightwave Technology. 2014;**32**:660-680. DOI: 10.1109/JLT.2013.2287219

[47] Liu Y, Hill M T, Calabretta N, Tangdiongga E, Geldenhuys R, Zhang S, Li Z, De Waardt H, Khoe G D and Dorren H J S: All-optical signal processing for optical packet switching

networks. In: Proceedings of SPIE; 15 September 2005; San Diego, California, USA; 2005, 59070J-1-12. DOI: 10.1117/12.621346

[48] Agrawal GP. Fiber-Optic Communication Systems. 4th ed. New York: Wiley; 2010. p. 603. ISBN: 978-0-470-50511-3

[49] Xuelin Y, Qiwei W, Weisheng H. High-speed all-optical long-term memory using SOA MZIs: Simulation and experiment. Optics Communication. 2012;**285**:4043-4047. DOI: 10.1016/j.optcom.2012.06.027

IntechOpen